Dongbo Xu, Werner Gillijns, Ling Ee Tan, David Rio, Max Delorme, Vicky Philipsen, Ryoung-han Kim, "Extend 0.33 NA extreme ultraviolet single patterning to pitch 28-nm metal design by low-n mask," J. Micro/Nanopattern. Mats. Metro. 21(4) 043202 (25 November 2022) https://doi.org/10.1117/1.JMM.21.4.043202

Extend 0.33 NA extreme ultraviolet single patterning to pitch 28-nm metal design by low-*n* mask

Dongbo Xu,[a,*] Werner Gillijns,[a] Ling Ee Tan,[a] David Rio,[b] Max Delorme,[b] Vicky Philipsen,[a] and Ryoung-han Kim[a]
[a]imec, Leuven, Belgium
[b]ASML Belgium, Leuven, Belgium

Abstract. Extending 0.33 NA extreme ultraviolet single patterning to 28-nm pitch becomes challenging in stochastic defectivity, which demands high-contrast lithographic images. The low-*n* attenuated phase-shift mask (attPSM) can provide superior solutions for individual pitches by mitigating mask three-dimensional effects. The simulation and experiment results have shown substantial imaging improvements: higher depth of focus at similar normalized image log slope and smaller telecentricity error values than the best binary mask configuration. In this work, the exploration of low-*n* attPSM patterning opportunity for pitch 28-nm metal design is investigated. Using generic building block features, the lithographic performance of the low-*n* attPSM is compared with the standard binary Ta-based absorber mask. In addition, the impact of mask tone (bright field (BF) versus dark field) on the pattern fidelity and process window is evaluated both by simulations and experiments. The results indicate that BF low-*n* attPSM provides the best patterning performance. Consequently, the BF low-*n* attPSM patterning performance is assessed with an actual imec N3 pitch 28-nm random logic metal design. The wafer data indicate BF low-*n* attPSM enables good patterning fidelity, as well as good overall process window with high exposure latitude (~20%). © *2022 Society of Photo-Optical Instrumentation Engineers (SPIE)* [DOI: 10.1117/1.JMM.21.4.043202]

Keywords: extreme ultraviolet single patterning; phase-shift mask; low-*n*; pitch 28 nm; logic metal.

Paper 22063G received Oct. 11, 2022; accepted for publication Nov. 10, 2022; published online Nov. 25, 2022.

1 Introduction

Currently, extreme ultraviolet lithography (EUVL) is part of high-volume manufacturing. Pushing the 0.33 NA EUV single patterning limits down to metal pitch 28 nm is becoming highly challenging in stochastic defectivity and process window. It is requiring complex and expensive design and mask and process co-optimization. Currently, imec is developing and evaluating patterning techniques to enable 0.33 NA EUV single patterning at pitch 28 nm.[1–4] To have good control of stochastic variability at tight pitch, high normalized image log slope (NILS) is required. However, mask three-dimensional (M3D) effects are known in EUVL imaging, to introduce lithographic image contrast fading, telecentricity errors through focus, and best focus shifts through pitch and through slit printability issues.[5–8] To mitigate the M3D effects, one approach is to employ alternative mask stacks.[7,9–17] The low-*n* attenuated phase-shift mask (attPSM) has shown substantial imaging improvements in simulations and experiments: a higher depth of focus (DoF) at similar NILS and a smaller telecentricity errors than the best binary mask configuration.[13,18–22] In this paper, the patterning of metal pitch 28-nm design using low-*n* attPSM mask technology is investigated in simulation and experimentally. The impact of the mask tone will also be considered. The standard binary Ta-based absorber masks (dark field (DF) and bright field (BF)) are used as the reference. The lithographic

*Address all correspondence to Dongbo Xu, dongbo.xu848@gmail.com

1932-5150/2022/$28.00 © 2022 SPIE

performance of the low-n attPSM for patterning pitch 28-nm metal design is evaluated using the first imec low-n attPSM masks (DF and BF masks).

The paper is organized in four core sections. Section 2 places this study within the broader picture of 0.33 NA EUV single patterning of pitch 28-nm metal layer. The source mask optimization (SMO) strategy and the MO results using the given low-n attPSM stack information will be briefly introduced in this section. Section 3 compares the lithographic patterning performance between the low-n attPSM and the reference binary mask by simulations and experiments for patterning vertical pitch 28-nm metal design based on generic building blocks. The findings have been reported in the conference paper.[21] Based on the finding in Sec. 3, Sec. 4 evaluates the BF low-n attPSM patterning performance of pitch 28-nm random logic metal design. Sec. 5 will provide the conclusions.

2 Context

In this paper, the simulations and experiments of the use-case are performed at conditions of imec's 0.33 NA NXE:3400 EUV scanner.[23] A negative tone development process is considered. All simulations were performed with ASML Tachyon.[24] The same SMO strategy in the paper of Xu et al.[17] was carried out together with the actual low-n attPSM stack provided by the maskshop (low-n and low-k absorber with $35 \sim 50$ nm) thickness[20] to obtain the optimized source for the low-n attPSM.

Figure 1 shows the optimized sources for binary mask and low-n attPSM, respectively, with a vertical 28-nm pitch 1:1 line/space (LS) grating as the SMO input target clip. These two sources are very similar with minor difference and will be used for all the simulations and experiments, for DF and BF mask tones, both for the low-n attPSM and the binary mask.

Figure 2 shows the imec N3 random logic design clip with design retargeting used in the MO steps with process window evaluation points placed at the red cutlines across the 1 μm^2 design area. Our previous investigation demonstrates that the low-n attPSM performs the best for 0.33 NA EUV single patterning of pitch 28 nm when using DF mask with subresolution assist features (SRAFs) and BF mask without SRAFs.[17]

Figure 3 shows the exposure latitude (EL) versus DoF of the critical dimension (CD)-based overall process window (OPW) for both DF mask with SRAFs and BF mask without SRAFs. An example of OPW is shown on the top right of the figure, which is calculated by overlapping the process window of each red cutline shown in Fig. 2, and an ellipse fit is used to compute the overall EL and DoF. With respect to the reference DF binary mask, the DF low-n attPSM with SRAFs shows a ~40% overall EL gain; and the BF mask without SRAFs allows ~25% overall EL gain compared to BF binary mask. In general, BF masks without SRAFs provides smaller overall DoF with respect to the DF mask with SRAFs.

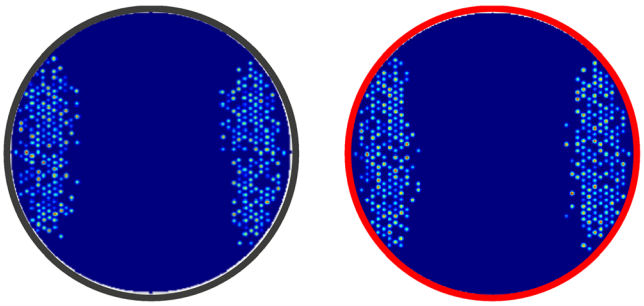

Fig. 1 SMO optimized sources when using vertical pitch 28-nm LS grating as the input target: the left figure shows the source of the reference binary mask, and the right figure shows the source for the low-n attPSM.

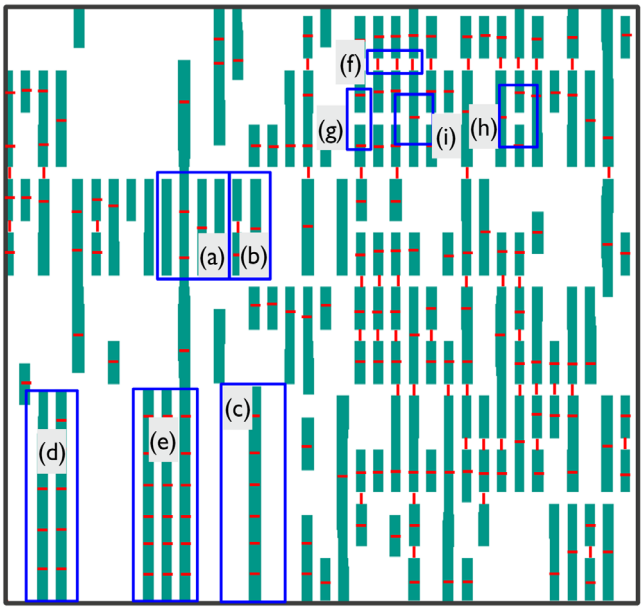

Fig. 2 Imec N3 random logic design clip with design retargeting: (a) dense LS at pitch 28 nm, (b) semidense LS, (c) isolated LS, (d) two-bar, (e) three-bar, (f) dense T2T with CD is 20 nm, (g) semi-dense T2T, (h) T2T between lines, and (i) line between T2Ts. Semi-isolated and isolated features target CD are between 14 and 18 nm. The red cutlines are used for OPW evaluation.

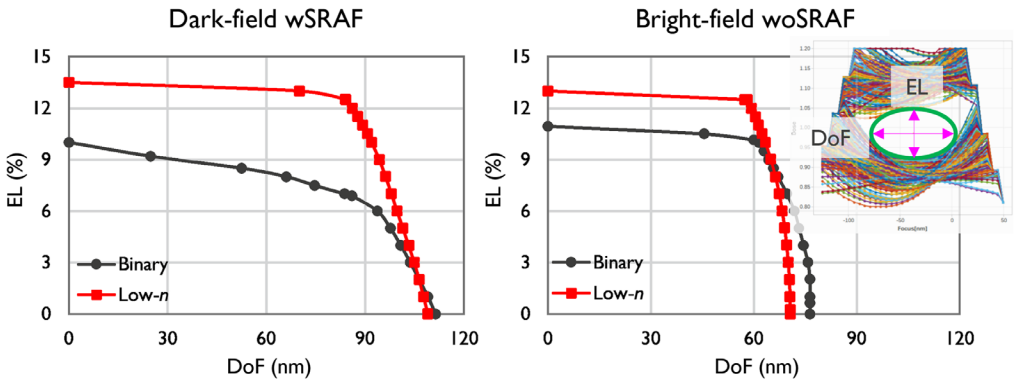

Fig. 3 EL versus DoF of CD-based overall OPW both for DF mask with SRAFs and BF mask without SRAFs. CD-based OPWs obtained with ±10% CD tolerance on trenches and ±20% CD tolerance on T2Ts.

3 Lithographic Performance Comparison Between Low-*n* AttPSM and Binary Mask

The imec N3 random logic design clip shown in Fig. 2 can be decomposed into several generic building blocks, such as:

1. dense LS, the pitch and target CD are 28 and 14 nm, respectively;
2. semidense and isolated LS with trench CDs varying between 14 and 18 nm;
3. two-bar and three-bar geometries with a minimum target resist line CD between the two/three bars of 14 nm;
4. Tip-to-tips (T2Ts) with a minimum T2T CD of 20 nm at pitch 28 nm.

Therefore, the patterning performance between the low-*n* attPSM and the reference binary mask is compared using these selected building blocks in this section: vertical LS, two-bar through slit, and T2T at pitch 28 nm with a minimum target T2T CD of 20n m. The side-lobe

printing risk will be assessed using the edge of pitch 28-nm LS grating. To clarify, the DF mask CD is the opening mirror CD, and the BF mask CD is the absorber CD in this paper.

3.1 *LS Through Pitch*

3.1.1 *Best focus shift*

The EUV-inherent M3D effects introduce best focus shifts through pitch. Figure 4 compares the process window-based best focus shift through pitch of the low-*n* attPSMs and the reference binary masks. The left figure shows the simulation results, and the right figure presents the experimental results obtained using imec's 0.33 NA NXE:3400 EUV scanner. The results show that the DF low-*n* attPSM has the largest best focus shifts through pitch, and the isolated LS results in 140-nm best focus shift with respect to the dense LS. The BF low-*n* attPSM has much smaller best focus shifts (~60 nm) with respect to the DF low-*n* attPSM and is similar to the DF and BF binary masks. Thus, the BF low-*n* attPSM as well as the reference binary masks could yield an OPW without considering SRAFs, and the OPWs of BF masks are shown in Fig. 3, more details of OPW comparisons are reported by Xu et. al.[17]

To mitigate the best focus shifts through pitch of the DF low-*n* attPSM, design retargeting and SRAF insertion are typically considered. Figure 5 shows the best focus shifts through mask CD of LS gratings at pitch 98 nm. The left figure highlights the simulation results and is to be compared with the right figure showing the corresponding wafer data. The large best focus shift of the DF low-*n* attPSM can be partly reduced by increasing the mask CD with a minimum best focus shift of ~50 nm (in absolute value) obtained from a 32-nm mask CD. However, as the

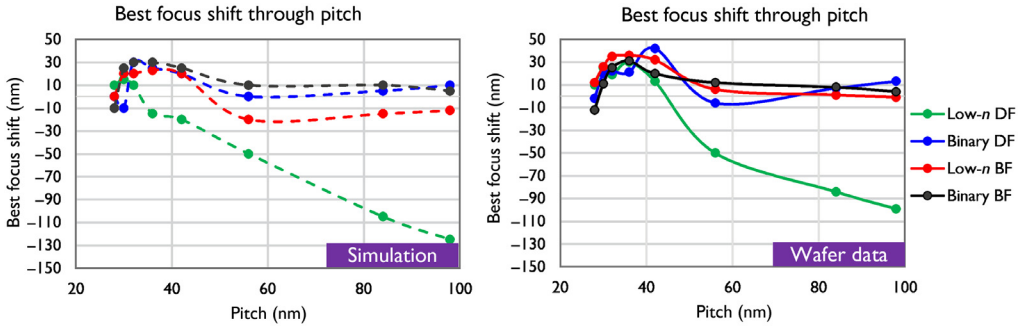

Fig. 4 Best focus shifts through pitch of the low-*n* attPSM and the reference binary mask. The left figure shows the simulation results, and the right figure presents the experimental results obtained from NXE:3400. The sources are shown in Fig. 1.

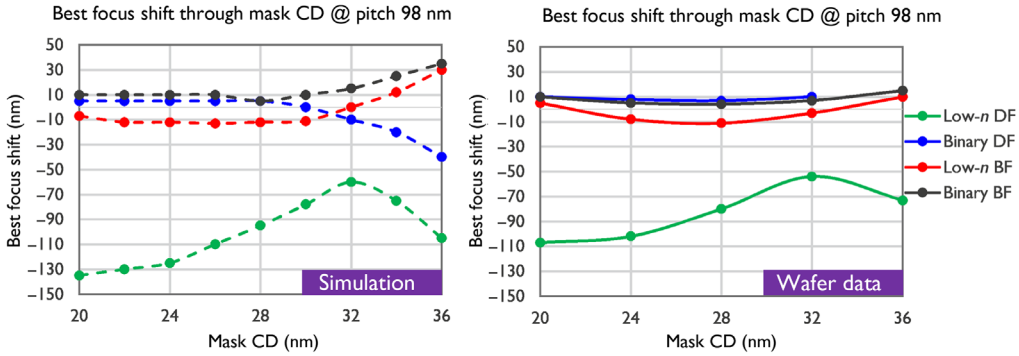

Fig. 5 Best focus shifts through mask CD of LS gratings at pitch 98 nm. The left figure shows the simulation results, and the right figure presents the experimental results obtained using a 0.33 NA NXE:3400 EUV scanner. The sources are shown in Fig. 1.

mask CD becomes larger, the best focus shift becomes larger again (in absolute value). Therefore, only considering the mask CD bias as unique knob to tune away the best focus shift appears to be insufficient. SRAF insertion is required as well.

Figure 6 shows the intensity profile distribution propagating through focus for LS grating at pitch 56 nm and mask CD 20 nm. The best focus of each case is defined by the center of the corresponding OPW. Comparing the four use cases shown in the Fig. 6, because of large best focus shifts through pitch of the DF low-n attPSM, the feature does not print at defocus $=$ -50 nm (i.e., the intensity profile does not reach the model threshold). When the intensity propagates further through focus, the simulation shows that the background intensity will exceed the model threshold and thus print on wafer. It is due to the interference between the diffraction light and background light. Therefore, mitigating this feature's best focus shift with SRAF placements turns out to be very challenging.

When considering SRAF insertion of the DF mask, overexposure is required to evaluate the SRAF printing risk. Figure 7 shows the relationship between overexposure latitude and SRAF CD at defocus in the range of -50 and $+50$ nm with step of 10 nm (simulation with an optical model). To avoid SRAF printing inside of the OPW, a certain EL through focus is needed. The top figure demonstrates that SRAF CD needs to be smaller than 6 nm in order for a reasonable EL through focus ($>10\%$) to be ensured. Unfortunately, this is contradicts the minimum value for SRAF imposed by the current mask rule check (MRC). Considering the current MRC of 8 nm for the minimum SRAF size, the circled points (in green) show a negative overexposure latitude at -30 nm defocus and a positive ($>30\%$) overexposure latitude at $+30$ nm defocus. In other words, this implies that the SRAFs with a CD of 8 nm will print on the wafer at -30 nm defocus, but will not print at +30 nm defocus with the nominal dose. The bottom figure illustrates the measured scanning electron microscope (SEM) images of LS pitch 56-nm mask CD 20 nm with 8-nm SRAF size through focus, SRAF starts printing at best focus condition. To avoid such an SRAF printing issue, design retargeting is preference for this feature.

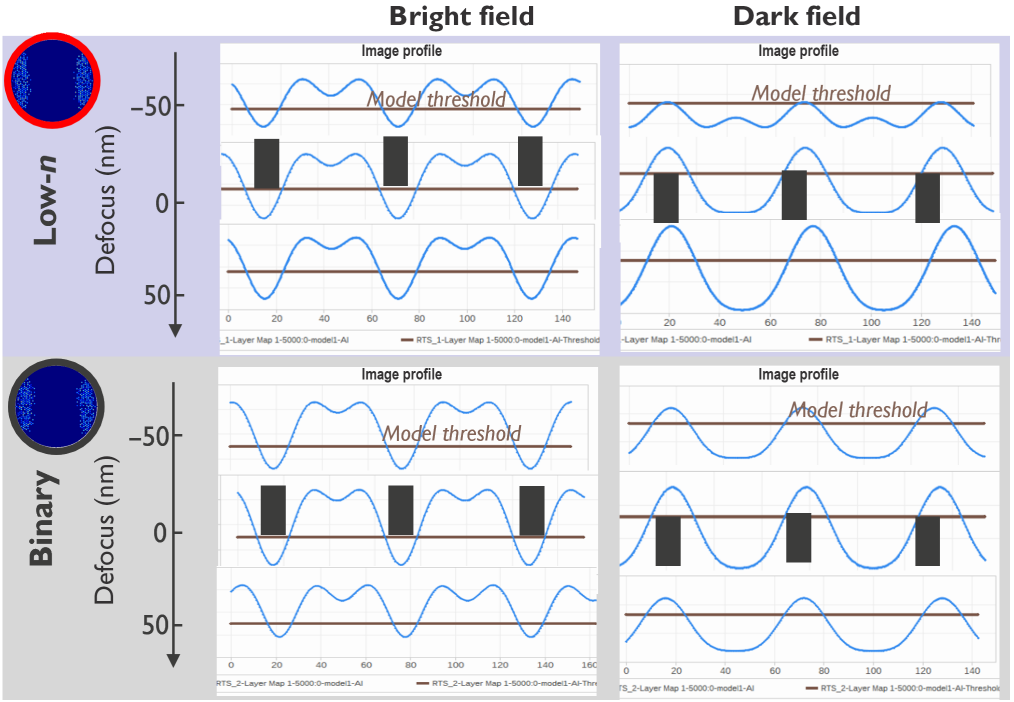

Fig. 6 Aerial image intensity profile distribution through focus for LS grating: pitch 56 nm, mask CD 20 nm. The best focus for each case is defined by the center of the corresponding OPW shown in Fig. 3.

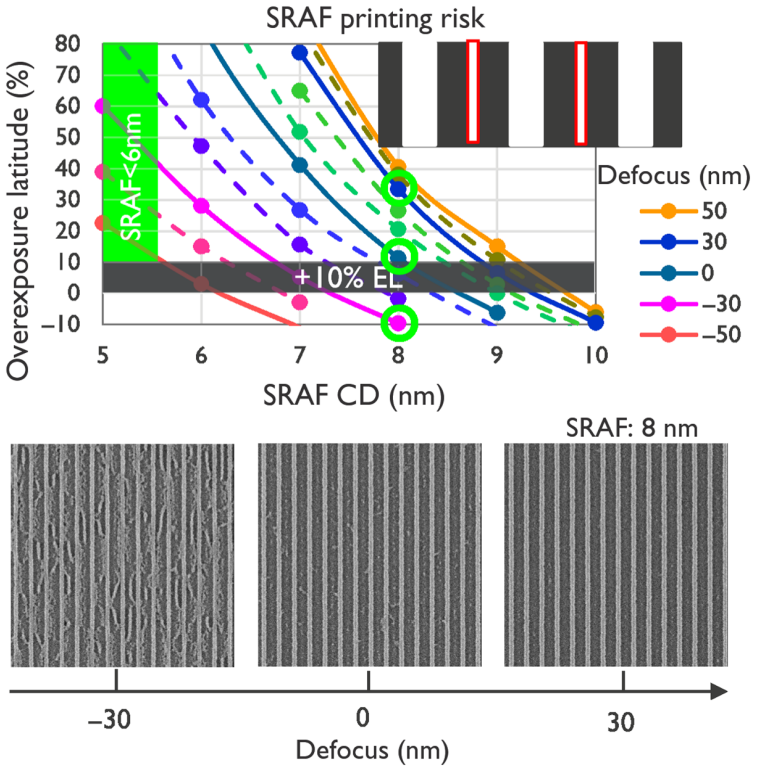

Fig. 7 The relationship between overexposure latitude and SRAF CD for LS grating: pitch 56 nm, mask CD 20 nm, and the highlighted three points using the circle are the EL of 8-nm SRAF at defocus −30, 0, and +30 nm, respectively.

3.1.2 *Normalized image log slope distribution*

Figure 8 shows the NILS distribution versus pitch/mask CD. The purple line defines a pattern density equal to 0.5, and the blue bounded area represents the pitch and mask CD distribution of the imec N3 pitch 28-nm relevant design. The left column is for the BF mask use case, and the NILS distribution is mainly driven by the mask CD. The BF low-n attPSM has a slightly better NILS for the dense LS with pitches smaller than 45 nm, whereas the forbidden pitch phenomena is slightly more noticeable around 45 to 55 nm pitch than in the BF binary mask case. The BF binary mask has good NILS distribution through pitch (>40 nm) with large mask CD (>20 nm). To pattern the iN3 pitch 28-nm relevant design, the BF low-n attPSM has slightly higher NILS with smaller mask CD with respect to the binary mask.

The right column is the DF mask use case. As shown in the figure, the mask tone has a significant impact on the NILS distribution (left and right image of each row). In the case of DF mask, the NILS distribution through pitch and mask CD is relatively similar. The NILS distribution of both DF masks has a clear transition region at the density ~0.5. The DF masks with large CD and higher pattern density (>0.5) allow for a higher NILS. There is a slight difference as the pitch and mask CD becomes larger. In general, for patterning the imec N3 pitch 28-nm relevant design, DF masks have lower NILS through pitch and mask CD with respect to the BF masks.

Considering the tightest pitch 28-nm LS grating, Fig. 9 displays the dose sensitivity and pattern printability of the BF masks comparison between low-n attPSM and the reference binary mask. The left figure is the dose sensitivity versus the mask CD at pitch 28 nm. The triangles are the current wafer anchors. The BF mask of the low-n attPSM has a slightly lower dose sensitivity (absolute value) with respect to the binary mask. The right figures are the line width roughness (LWR) comparison through focus for different doses, for both the BF low-n attPSM and the BF binary masks. The BF low-n attPSM slightly improves the LWR with respect to the BF binary mask.

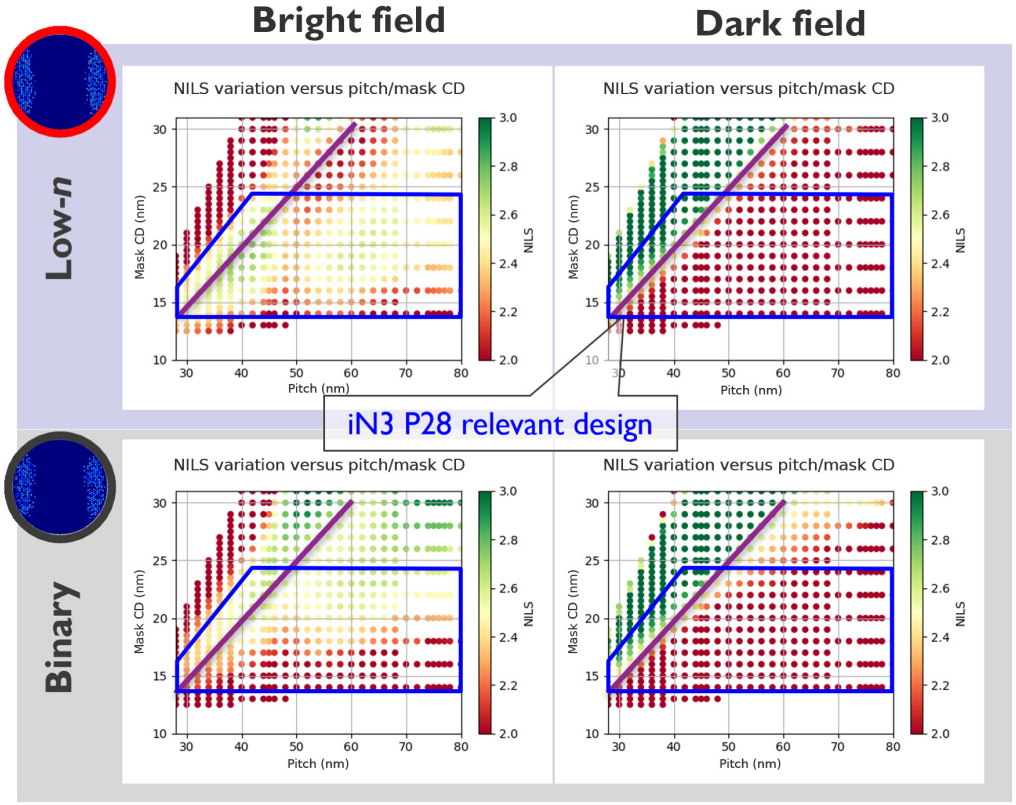

Fig. 8 NILS distribution versus pitch/mask CD. The blue rectangle is pitch and mask CD distribution of the iN3 relevant design pattern.

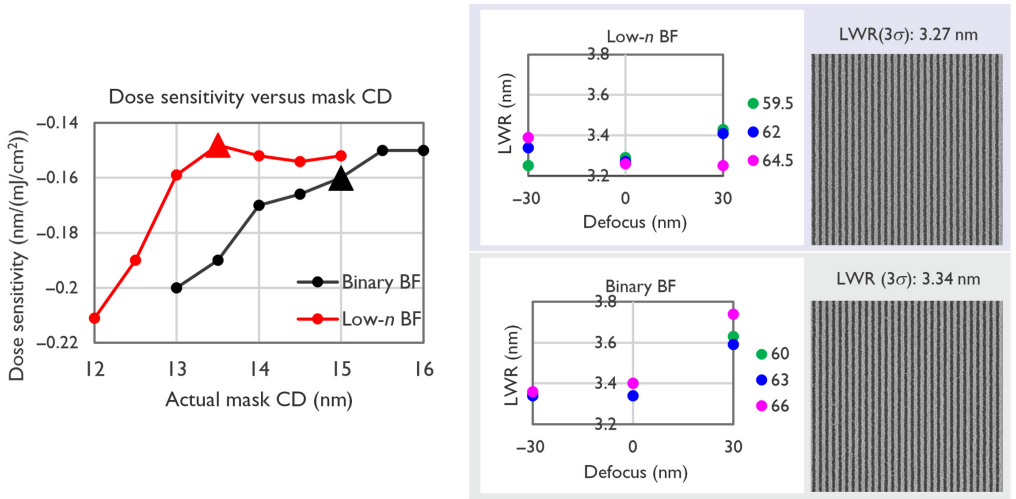

Fig. 9 Dose sensitivity and pattern printability of the BF masks comparison between BF low-*n* attPSM and the reference binary BF mask, for patterning dense pitch 28-nm LS gratings, LWR is not measured by best known method, and only for comparison purpose.

3.2 *Two-Bar Printability*

3.2.1 *Two-bar pitch 28 nm*

Our study shows that one of the main hotspots for pitch 28-nm random logic design is the two-bar like feature with a pitch of 28 nm. The left figure of Fig. 10 illustrates an example of a design

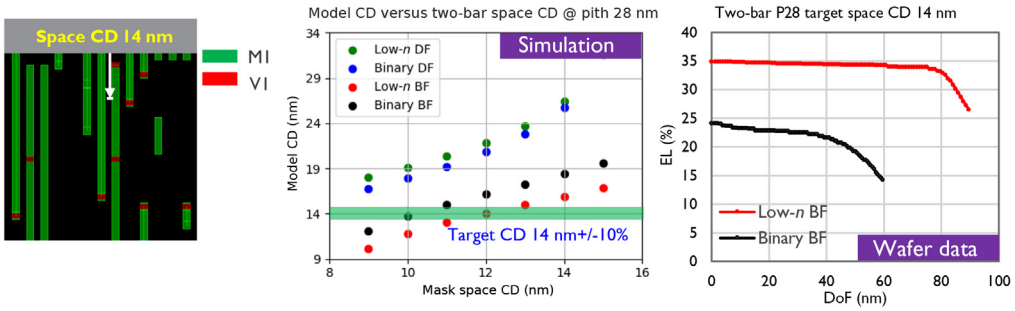

Fig. 10 Two-bar printability at pitch 28-nm for target resist line CD 14 nm of low-*n* attPSM and binary mask with different tone.

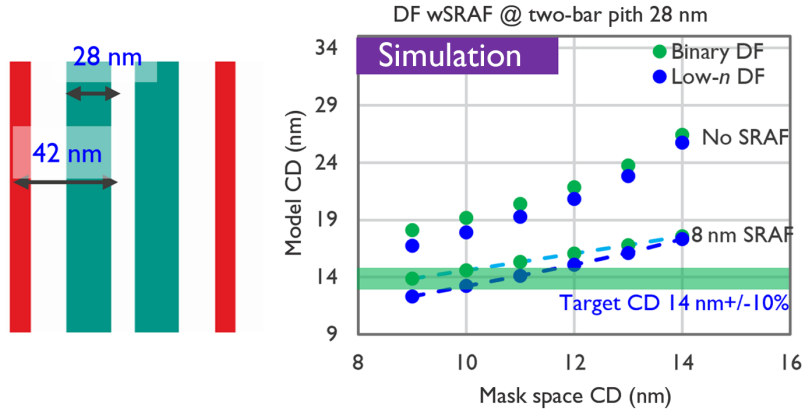

Fig. 11 Simulated CD versus the mask space CD in between the two-bar of pitch 28 nm without and with 8-nm SRAFs.

clip, and the position marked by the white arrow is an example of the previously mentioned pitch 28-nm two-bar kind of design where the vias are landing on top of the metal lines. The width of the metal lines (resist trench) and the distance (resist line, mask space CD) between two metal lines are both 14 nm. To have a good patterning quality, the two metal lines can be retargeted, but doing the same for the distance between these two metal lines tends to be more difficult, due to the constraint of the vias landing on top. Therefore, the process must print 14-nm resist line between these two resist trenches. The middle figure presents the simulated CD versus the mask space CD in between two-bar of pitch 28 nm. The green rectangle represents the target 14 nm $\pm$ 10% CD variation. Without considering SRAFs, the simulations indicate that only BF masks can print resist line 14 nm on target, and the BF low-*n* attPSM can use slightly larger mask space CD ($\sim$12 nm) than the BF binary mask ($\sim$10 nm) to print the target resist line CD 14 nm. The right figure is the measured EL versus DoF of BF masks of target resist line CD 14 nm with $\pm$10% CD variation for low-*n* attPSM and binary mask. The EL and DoF of the BF low-*n* attPSM are improved by $\sim$40% with respect to the binary BF mask.

To enable the DF mask for printing target resist line CD 14 nm, SRAF insertion should be considered. Figure 11 shows the simulated CD vs. the space CD in between two-bar of pitch 28 nm without SRAF and with 8-nm SRAFs. The positions of SRAFs are shown in the left figure. By inserting SRAFs, both DF low-*n* attPSM and DF binary mask are able to print the target resist line CD 14 nm with the mask space CD 11 nm in between the two-bar.

3.2.2 *Two-bar through slit*

Figure 12 compares the impact of M3D effects on the CD difference through slit of vertical two-bar pitch 40-nm CD 20 nm. The left figure presents the simulated left bar and right bar CD difference. Both DF and BF binary masks show similar small CD difference through slit

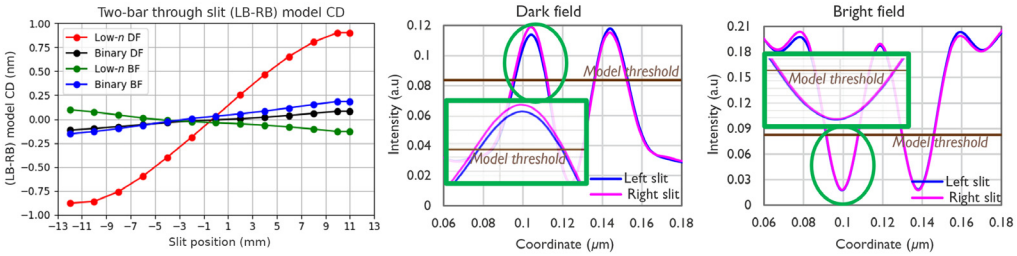

Fig. 12 The comparison of pitch 40-nm vertical two-bar through slit impact (left), and the intensity profile at the left and right edge of the slit for both DF and BF of low-*n* attPSM.

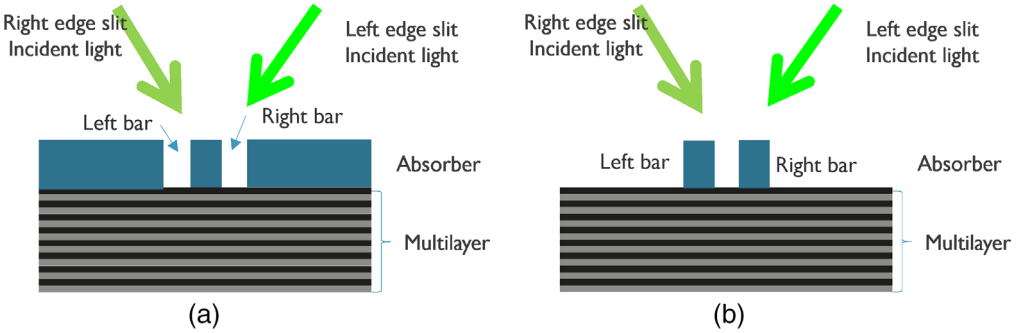

Fig. 13 The schematics of the incident light of the two-bar at the left slit and right slit: (a) DF mask and (b) BF mask.

($-0.25 \sim 0.25$ nm). The BF low-*n* attPSM has similar CD difference with an opposite trend through slit with respect to the binary masks. However, the DF low-*n* attPSM exhibits a larger CD difference through slit ($-1 \sim 1$ nm). The middle and right figures in Fig. 12 show the intensity profile at the left and right edge of the slit for both DF and BF low-*n* attPSM of the two-bar. The low-*n* attPSM DF mask introduces a pronounced intensity imbalance at the edge of the slit with respect to the BF mask, which results in the larger CD difference. Therefore, through slit aware OPC should be considered for DF low-*n* attPSM.

To have a better understanding of such effects through slit, Fig. 13 shows the schematic of the incident light direction of the two-bar at left and right edge of the slit for both DF and BF masks. The Ta-based absorber binary mask has reflectivity ~2%, and the low-*n* attPSM absorber has reflectivity in the range of 8% and 15%,[20] which has four to seven times more reflectivity than Ta-based absorber. Considering the DF masks [cf. Fig. 13(a)] and the two-bar placed at the left slit edge, the incident light on the left bar is partly blocked by the thin absorber extension (in *x*-axis) between these two bars, and the right bar is partly stopped by the thick absorber extension (in *x*-axis) on the right side. Due to the thin absorber extension (in *x*-axis) between these two bars and the high reflectivity of the low-*n* absorber, the left bar of the DF low-*n* attPSM results in higher amount of the reflective light than the right bar, (see Fig. 12 middle plot, the intensity amplitude of the left slit is larger). The two-bar on the right slit edge shows the opposite. For the BF mask [cf. Fig. 13(b)], the two bars get similar amount of the light, and the M3D effects are less pronounced (see Fig. 12 right plot, the impact can be neglected).

3.3 *T2T Printability*

The imec N3 pitch 28-nm metal design rule allows aggressive T2T design with the minimum T2T CD being 20 nm. Figure 14 shows the simulated and experimental T2T printability at pitch 28 nm of low-*n* attPSMs and binary masks for different mask tones using the sources in Fig. 1, which are not optimized to print this tight T2T. The simulation results show that to print the target T2T CD of 20 nm, the mask T2T CD of the DF mask (both low-*n* attPSM and binary mask) needs to be around 10 nm, whereas of the BF low-*n* attPSM and binary mask needs to be around 20 and 25 nm, respectively. The wafer data in the middle figure show DF masks cannot

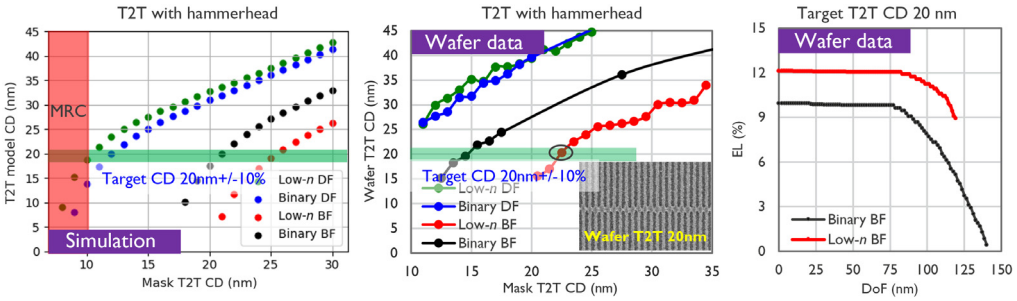

Fig. 14 T2T printability at pitch 28 nm of low-*n* attPSM and binary mask with different tonality.

print T2T CD with 20 nm on wafer, due to a large T2T pull back with respect to the aerial image simulation results. Instead, the BF masks can print target T2T CD 20 nm. The right figure displays the corresponding measured EL versus DoF for printing target T2T CD 20 nm with ±10% CD variation. The BF low-*n* attPSM shows an EL improvement of roughly 20% with respect to the binary BF mask. Figure 14 demonstrates that BF low-*n* attPSM delivers the best performance for T2T printing, which enables large mask T2T CD to print smaller target T2T CD on the wafer with higher EL. This will allow a better OPC convergence.

3.4 *Side-Lobe Printing*

Since the low-*n* attPSM has a higher reflectivity than the Ta-based binary mask, the side-lobe printing risk is higher for low-*n* attPSM masks and thus should be evaluated. Figure 15 shows the aerial image intensity profile distribution at the edge of pitch 28-nm LS grating. The model threshold for each case is determined during the MO flow based on the design clip shown in Fig. 2. The left results of BF masks in Fig. 15 indicate that the minimum background intensity of BF masks is larger than the maximum intensity of the pitch 28-nm LS main pattern. Lowering the exposure dose will increase the side-lobe printing risk; however, the main features will stop printing earlier. In other word, there is no side-lobe printing issue for BF masks. For the DF case, Fig. 15 shows the background intensity of the reference binary mask is zero, and thus, we do not have the side-lobe printing issue. However, the background intensity of the low-*n* attPSM is between the minimum and maximum intensity of the pitch 28-nm LS pattern, which means the DF low-*n* attPSM might yield side-lobe printing. The simulation shows that 82.1% overexposure

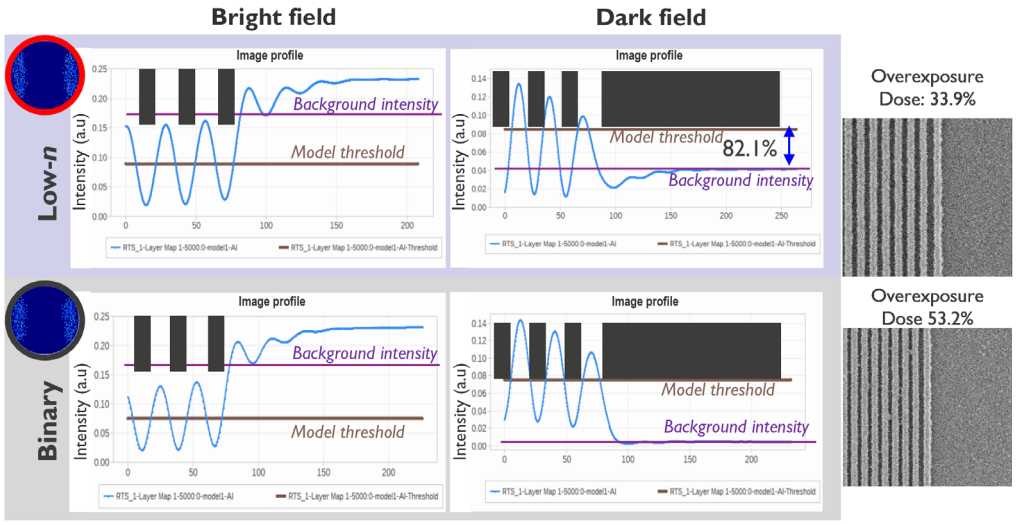

Fig. 15 Aerial image intensity profile distribution at the edge of pitch 28-nm LS building block at nominal condition, and the measured SEM images of DF low-*n* attPSM with 33.9% and 53.2% overexposure dose, respectively.

	Low-*n*		Binary	
	Dark field	Bright field	Dark field	Bright field
Best focus shift	Large	Small	Small	Small
Need SRAF	Yes (printing risk)	No	No	No
iN3 P28 relevant design NILS	Medium	High	Medium	High
P28 two-bar printing 14 nm resist line	Yes (+SRAF)	Yes	Yes(+SRAF)	Yes
M3D effects through slit (two-bar)	Pronounced	No	No	No
P28m T2T target 20 nm	Aggressive MRC	Yes	Aggressive MRC	Yes
Side-lobe print	No	No	No	No

Fig. 16 Comparative summary table of the improvement when using low-*n* attPSM and binary mask (green: ++; light green: +; and yellow: –).

dose is needed to get the background intensity touching the model threshold. The measured SEM images on the right side of the figure show that it is hard to see the side-lobe print at 33.9% overexposure dose, and only some speckles start appearing at 53.2% overexposure dose whereas at the same time, the main features start merging. Therefore, there is no side-lobe printing risk of DF low-*n* attPSM within the OPW for patterning metal layers.

3.5 *Executive Summary*

In this section, the patterning performance of low-*n* attPSMs and binary masks is compared using simulations as well as experimental data with a set of optimized sources for the selected generic building blocks. The impact of mask stack and tone is evaluated on the best focus shift through pitch, two-bar through slit, and the capability of printing two-bar and target T2T CD 20 nm at pitch 28 nm, as well as the side-lobe printing risk. The comparative table in Fig. 16 summarizes the improvement of each metric when using these four mask candidates.

To apply the DF low-*n* attPSM for patterning pitch 28-nm metal design, the mitigation of the large best focus shift through pitch requires design retargting and SRAFs insertion during OPC. However, the DF low-*n* attPSM has a potential SRAF printing risk (or requires more aggressive MRC). Therefore, SRAF insertion becomes very challenging. Notably, both DF low-*n* attPSM and binary masks could not print target 20-nm T2T at pitch 28 nm with the current sources, and SRAF insertion is necessary for patterning two-bar at the same pitch with a 14-nm resist line in the middle. In general, the DF low-*n* attPSM has slightly worse performance with respect to the reference DF binary mask. Compared with the DF low-*n* attPSM, the BF low-*n* attPSM has smaller best focus shifts through pitch and higher NILS for pitch 28-nm relevant design. Also, SRAFs are not needed to print 14-nm resist line in the middle of pitch 28-nm two-bar. Moreover, the BF low-*n* attPSM can print target T2T CD 20 nm with large mask T2T CD. With respect to the BF binary mask, the BF low-*n* attPSM delivers better patterning performance of two-bar and T2T CD 20 nm at pitch 28 nm. In general, the BF low-*n* attPSM has the best patterning performance with respect to the other three cases.

4 OPW Evaluation of Random Logic Metal Design at Pitch 28 nm for BF Low-*n* attPSM

The imec N3 random logic design clip shown in Fig. 2 with different OPC flavors and 40× repetitions of each OPC flavor have been placed on the low-*n* attPSMs. Notably, because this is our first low-*n* mask, the OPCs were run with optical model only, and thus, the resist proximity effects were not taken into account. Therefore, the patterning study in this section focuses on evaluating the OPW and patterning quality of the random logic metal design clip on the BF low-*n* attPSM.

Figure 17 presents the printability of pitch 28-nm random logic metal design clip through dose at best focus and through focus at the best dose in the top and bottom row, respectively.

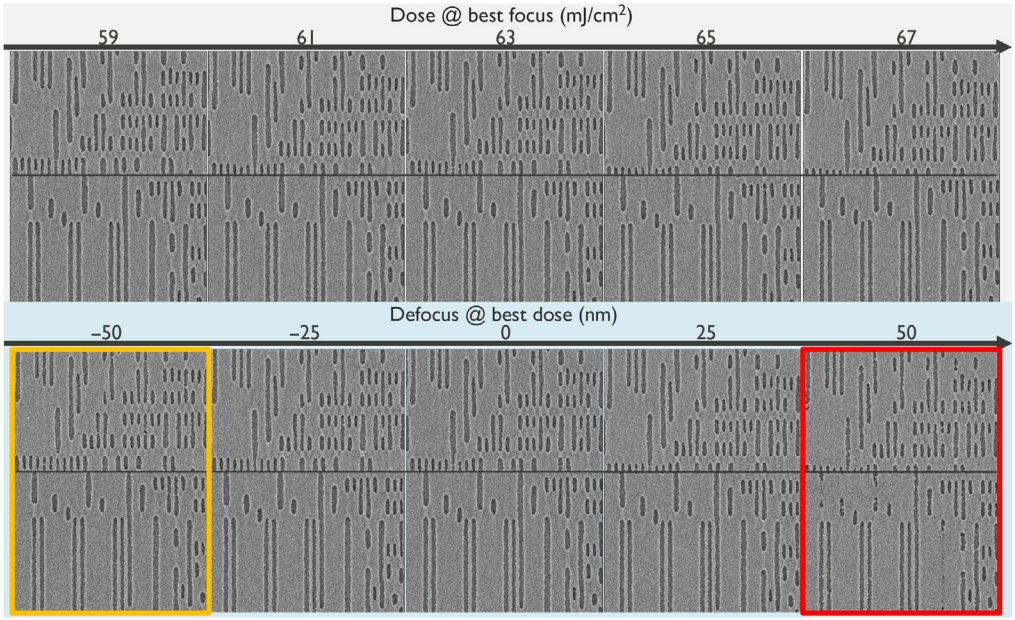

Fig. 17 Random logic design printability through dose at best focus (top row) and through focus at the best dose (bottom row), respectively. Bottom row: the left image (in orange) has larger LWR, and the right image (in red), isolated LS stop printing.

Considering the dose range of ±6% and focus range of ±50 nm, pitch 28-nm random logic metal clip has good printability through dose, whereas slightly worse printability through focus. It seems that the LWR becomes larger as the absolute defocus becomes larger (left and right images of the bottom row), and the isolated LS is not printing (right image of the bottom row). To quantify the patterning quality, ASML MXP tool[25,26] is used to extract the CD gauges, as well as the CD variation across the focus exposure matrix on the wafer.

4.1 *OPW Evaluation*

Figure 18 displays the wafer CD measurement flow using MXP to extract CD-based OPW: first, 40× repetitions of the random logic metal design clip are measured by 2 parts: the dense area and the more isolated area; second, 20 raw images of each area are measured at each dose and focus condition; third, MXP is used to obtain the average image and contour; and last, measurement boxes are placed across the clips, and the measured CD at each position is extracted by averaging the measured CDs in the measured box.

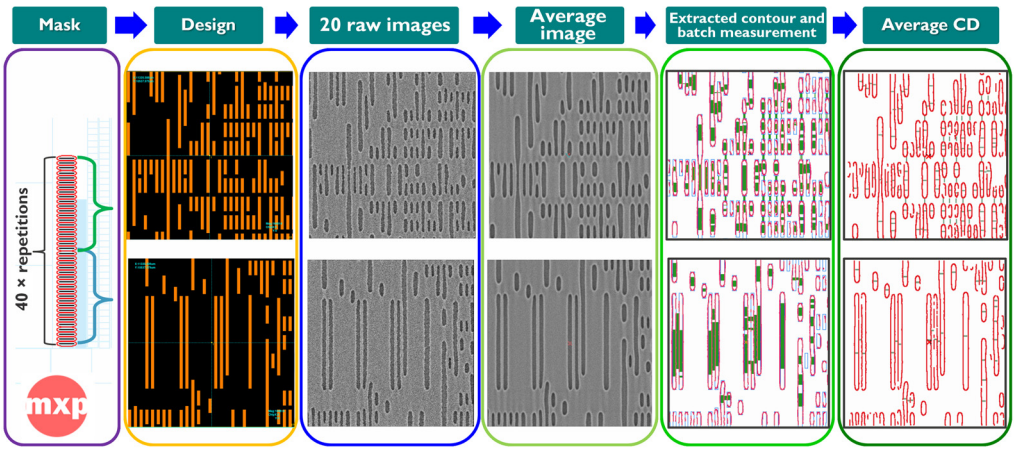

Fig. 18 MXP flow of imec N3 pitch 28-nm random logic design clip CD measurement.

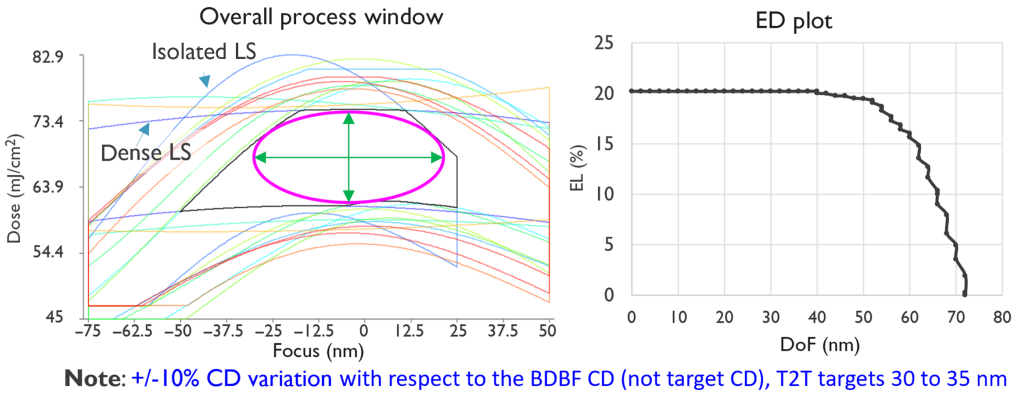

Fig. 19 OPW of pitch 28-nm random logic metal design clip.

Figure 19 shows the OPW of the measured two clips where the main features shown in Fig. 2 are measured. To clarify, the OPW is defined by $\pm 10\%$ CD variation with respect to the best dose best focus (BDBF) condition, and the T2T is printing at 30 to 35 nm due to the resist proximity effect. The BF low-n attPSM is able to deliver good OPW with high EL (~20%). The DoF limiter of the OPW is the best focus shift between dense LS and isolated trenches. To obtain a larger DoF, design CD retargeting of isolated features or dummy metal insertion is necessary.

4.2 *Printability*

Besides a good OPW, the good printability within OPW is very important to sustain the yield, delivering high resolution and defect-free processes. Therefore, the stochastic phenomena must be quantified. Neureuther and Willson[27] have specified the shot noise limit, i.e., the limit where stochastic effects become important, for x-ray lithography as 1000 photons within a volume element of CD/4. Thus, a corresponding length scale of imec N3 pitch 28-nm design with CD of 14 nm is 3.5 nm.

Figure 20 shows the clip's printability quantification flow. Compared with Fig. 18, here the raw image contours are extracted and the CD variation band (3σ of CDs) is measured to quantify

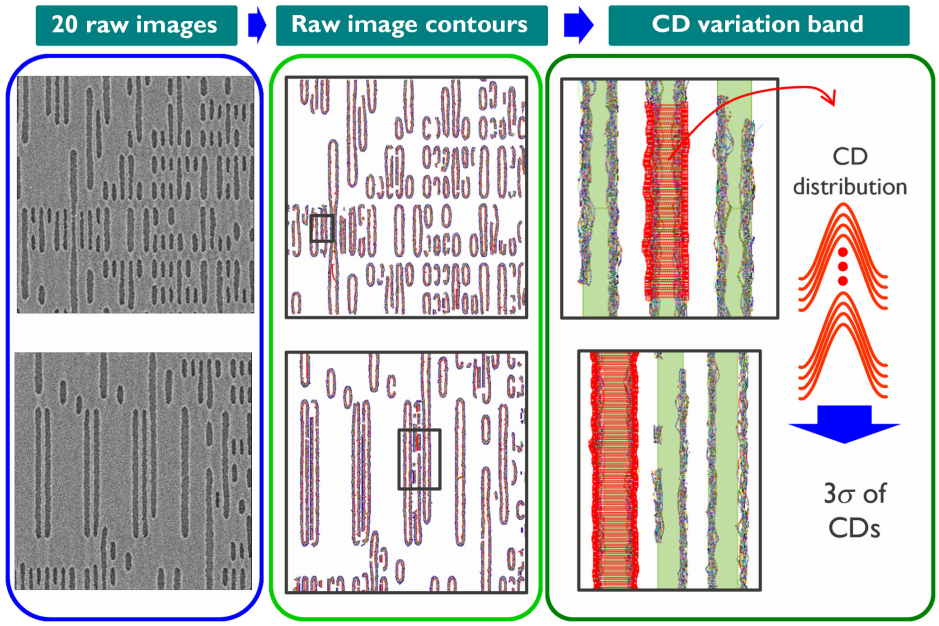

Fig. 20 MXP flow of imec N3 pitch 28-nm random logic design clip printability measurement.

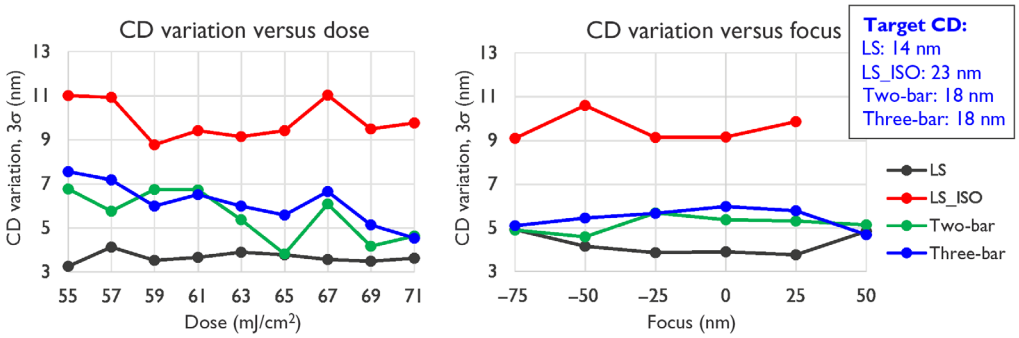

Fig. 21 Main features CD variation within OPW.

the stochastic effect. Figure 21 shows the BF low-*n* attPSM CD variation through dose at the best focus and through focus at the best dose, which indicates that isolated LS have the largest CD variation, whereas the dense LS have smallest CD variation. The CD variation versus Dose on the left displays decreasing CD variations of two-bar and three-bar as the dose increases; but no clear trend for LS_ISO and dense LS, this is due to the measured CDs becomes smaller with increasing dose. The CD variation of dense LS at BDBF is ~3.5 nm, which roughly meets the required 3.5-nm length scale. However, the mitigation strategy of large CD variation of the isolated LS is becoming necessary.

5 Conclusion

In this paper, the exploration of the use of low-*n* attPSMs for 0.33 NA EUV single patterning opportunity of pitch 28-nm metal design has been investigated. The patterning performance of low-*n* attPSMs is compared with the standard binary masks using selected metrics: best focus through pitch, two-bar through slit, and two-bar and T2T at pitch 28 nm. The mask tone (DF versus BF) is also considered. The simulation and wafer data indicate that the BF low-*n* attPSM enables the best patterning performance among all the four combinations. Afterwards, the patterning performance of the BF low-*n* attPSM is assessed by the imec N3 use case to pattern an imec N3 pitch 28-nm random logic metal design clip. The BF low-*n* attPSM enables good OPW with high EL (~20%), and the OPW is limited by the best focus shift between dense and isolated LS. Because aggressive MRC (<6 nm) is needed for BF mask to insert SRAFs,[17] design CD retargetting or dummy metal insertion is becoming necessary for isolated features. Generally, BF low-*n* attPSM shows very promising performance for extending 0.33 NA EUV single patterning down to pitch 28-nm metal design.

Furthermore, BF mask quality is studied at imec. To enable BF mask patterning these tight pitch and aggressive T2T, prioritization of the absorber mask features is required to bring BF EUV mask quality to be on par with EUV DF mask quality. To prepare for high-NA EUVL, the alternative mask quality and pattering performance will be further assessed.

Acknowledgments

The authors would like to acknowledge the contributors at imec: Jeroen Van de Kerkhove, Tatiana Kovalevich, Lieve van Look, Jae Uk Lee, and TMA team.

References

1. D. Xu et al., "EUV single patterning exploration for pitch 28 nm," *Proc. SPIE* **11614**, 116140Q (2021).
2. D. Rio et al., "Extending 0.33 NA EUVL to 28 nm pitch using alternative mask and controlled aberrations," *Proc. SPIE* **11609**, 116090T (2021).

3. J.-H. Franke et al., "Metal layer single EUV expose at pitch 28 nm: how bright field and NTD resist advantages align," *Proc. SPIE* **11609**, 116090R (2021).
4. D. D. Simone et al., "28 nm pitch single exposure patterning readiness by metal oxide resist on 0.33NA EUV lithography," *Proc. SPIE* **11609**, 116090Q (2021).
5. A. Erdmann et al., "Mask-induced best-focus shifts in deep ultraviolet and extreme ultraviolet lithography," *J. Micro/Nanolithogr. MEMS MOEMS* **15**, 021205 (2016).
6. A. Erdmann et al., "Characterization and mitigation of 3D mask effects in extreme ultraviolet lithography," *Adv. Opt. Technol.* **6**, 187–201 (2017).
7. V. Philipsen et al., "Reducing EUV mask 3D effects by alternative metal absorbers," *Proc. SPIE* **10143**, 1014310 (2017).
8. J.-H. Franke et al., "Improving exposure latitudes and aligning best focus through pitch by curing M3D phase effects with controlled aberrations," *Proc. SPIE* **11147**, 111470E (2019).
9. M. Burkhardt, "Investigation of alternate mask absorbers in EUV lithography," *Proc. SPIE* **10143**, 1014312 (2017).
10. V. Philipsen et al., "Novel EUV mask absorber evaluation in support of next-generation EUV imaging," *Proc. SPIE* **10810**, 108100C (2018).
11. J. Finders et al., "Experimental investigation of a high-k reticle absorber system for EUV lithography," *Proc. SPIE* **10957**, 1095714 (2019).
12. R. Sejpal et al., "Exploring alternative EUV mask absorber for iN5 self-aligned block and contact layers," *Proc. SPIE* **11148**, 111481B (2019).
13. A. Erdmann et al., "Perspectives and tradeoffs of absorber materials for high NA EUV lithography," *J. Micro/Nanolithogr. MEMS MOEMS* **19**(4), 041001 (2020).
14. V. Philipsen, "Mask is key to unlock full EUVL potential," *Proc. SPIE* **11609**, 1160904 (2021).
15. M. Wu et al., "Study of novel EUVL mask absorber candidates," *J. Micro/Nanopatterning Mater. Metrol.* **20**(2), 021002 (2021).
16. D. Xu et al., "Exploration of alternative mask for 0.33NA EUV single patterning at pitch 28nm," *Proc. SPIE* **11854**, 118540T (2021).
17. D. Xu et al., "Exploration of alternative mask for 0.33NA extreme ultraviolet single patterning at pitch 28-nm metal design," *J. Micro/Nanopatterning Mater. Metrol.* **21**(2), 024401 (2022).
18. A. Erdmann et al., "Attenuated PSM for EUV: can they mitigate 3D mask effects?" *Proc. SPIE* **10583**, 1058312 (2018).
19. M.-C. van Lare, F. J. Timmermans, and J. Finders, "Alternative reticles for low-k1 EUV imaging," *Proc. SPIE* **11147**, 111470D (2019).
20. C. van Lare et al., "Investigation into a prototype extreme ultraviolet low-n attenuated phase-shift mask," *J. Micro/Nanopatterning Mater. Metrol.* **20**(2), 021006 (2021).
21. D. Xu et al., "Investigation of low-n mask in 0.33 NA EUV single patterning at pitch 28 nm metal design," *Proc. SPIE* **12051**, 120510H (2022).
22. A. Erdmann, H. Mesilhy, and P. Evanschitzky, "Attenuated phase shift masks: a wild card resolution enhancement for extreme ultraviolet lithography?" *J. Micro/Nanopatterning Mater. Metrol.* **21**(2), 020901 (2022).
23. M. van de Kerkhof et al., "Enabling sub-10 nm node lithography: presenting the NXE:3400B EUV scanner," *Proc. SPIE* **10143**, 101430D (2017).
24. S. Hsu et al., "EUV resolution enhancement techniques (RETs) for k1 0.4 and below," *Proc. SPIE* **9422**, 94221I (2015).
25. W. Yuan et al., "Metrology and deep learning integrated solution to drive OPC model accuracy improvement," *Proc. SPIE* **10961**, 109610N (2019).
26. Y.-S. Kim et al., "OPC model accuracy study using high volume contour based gauges and deep learning on memory device," *Proc. SPIE* **10959**, 1095913 (2019).
27. A. R. Neureuther and C. G. Willson, "Reduction in x-ray lithography shot noise exposure limit by dissolution phenomena," *J. Vac. Sci. Technol. B* **6**(1), 167–173 (1988).

Dongbo Xu is working as an R&D engineer at imec. He received his ME from the University of Chinese Academy of Sciences. He was pursuing a PhD in Fraunhofer IISB Computational

Lithography and Optics Group, Erlangen and received his PhD in the field of computational lithography from Friedrich-Alexander-University Erlangen-Nürnberg in 2016. His research interests include optical and EUV lithography simulation, OPC modeling and image processing with machine learning.

Werner Gillijns is currently OPC team lead at imec. He has been active in computational lithography and imaging for over ten years at imec. He received his PhD in physics at the Catholic University of Leuven, Belgium, in 2008. In 2004, he completed his master's degree in physics at the Catholic University of Leuven. His fields of interest include computational lithography, especially OPC modeling, automation, CDSEM metrology, and machine learning.

Biographies of the other authors are not available.